Video Article

Quantifying Leukocyte Egress Via Lymphatic Vessels from Murine Skin and Tumors

Maria M. Steele[1], Madeline J. Churchill[2], Alec P. Breazeale[1], Ryan S. Lane[1], Nicholas A. Nelson[1], Amanda W. Lund[1,2,3,4]

[1]Department of Cell, Developmental, & Cancer Biology, Oregon Health and Science University

[2]Department of Molecular Microbiology & Immunology, Oregon Health and Science University

[3]Department of Dermatology, Oregon Health and Science University

[4]Knight Cancer Institute, Oregon Health and Science University

Correspondence to: Amanda W. Lund at lunda@ohsu.edu

URL: https://www.jove.com/video/58704
DOI: doi:10.3791/58704

Keywords: Lymphatic vessels, egress, trafficking, Kaede, FITC paint, leukocytes, melanoma

Date Published: 11/28/2018

Citation: Steele, M.M., Churchill, M.J., Breazeale, A.P., Lane, R.S., Nelson, N.A., Lund, A.W. Quantifying Leukocyte Egress Via Lymphatic Vessels from Murine Skin and Tumors. *J. Vis. Exp.* (), e58704, doi:10.3791/58704 (2018).

Abstract

Leukocyte egress from peripheral tissues to draining lymph nodes is not only critical for immune surveillance and initiation but also contributes to the resolution of peripheral tissue responses. While a variety of methods are used to quantify leukocyte egress from non-lymphoid, peripheral tissues, the cellular and molecular mechanisms that govern context-dependent egress remain poorly understood. Here, we describe the use of *in situ* photoconversion for quantitative analysis of leukocyte egress from murine skin and tumors. Photoconversion allows for the direct labeling of leukocytes resident within cutaneous tissue. Though skin exposure to violet light induces local inflammatory responses characterized by leukocyte infiltrates and vascular leakiness, in a head-to-head comparison with transdermal application of fluorescent tracers, photoconversion specifically labeled migratory dendritic cell populations and simultaneously enabled the quantification of myeloid and lymphoid egress from cutaneous microenvironments and tumors. The mechanisms of leukocyte egress remain a missing component in our understanding of intratumoral leukocyte complexity, and thus the application of the tools described herein will provide unique insight into the dynamics of tumor immune microenvironments both at steady state and in response to therapy.

Video Link

The video component of this article can be found at https://www.jove.com/video/58704/

Introduction

Peripheral tissue immune responses are shaped not only by leukocyte recruitment to the sites of inflammation but also by mechanisms that regulate their subsequent retention. Thus, protective immunity is dictated by cumulative cellular and molecular mechanisms that determine whether a leukocyte enters, stays within, or rather migrates out of peripheral tissue via lymphatic vessels. Importantly, the propensity for leukocytes to exit tissue through lymphatic vessels (termed egress) is linked to their specialized functions. Dendritic cells (DC) acquire migratory behavior in response to maturation signals leading to antigen transport and presentation in draining lymph nodes (dLN), a process that is necessary for adaptive immunity[1]. Scavenging myeloid cells, such as macrophages and neutrophils, serve to clear apoptotic debris through phagocytosis. During bacterial infection, neutrophils egress tissue and ultimately undergo apoptosis in dLNs[2] and in a model of DSS-induced colitis, data supports the hypothesis that macrophage egress is necessary to resolve local inflammation[3]. Whether neutrophil and macrophage egress occurs in all inflammatory contexts, however, is unknown. Evidence for T lymphocyte egress from steady state[4,5,6,7], infected[8], and inflamed[4,9,10,11,12] peripheral, non-lymphoid tissues indicates that T cells actively recirculate, though the tissue-based signals that drive this exit remain poorly understood. Several studies have identified signals necessary for directional migration towards draining lymphatic capillaries and subsequent egress including chemokine (C-C motif) ligand 21 (CCL21) and its receptor CCR7[4,11,13], chemokine (C-X-C motif) ligand 12 (CXCL12) and its receptor CXCR4[2,14], and sphingosine-1-phosphate (S1P)[10,15,16]. These mechanisms are not active in all contexts, however, and whether they determine egress of all cell types remains an open question. Importantly, further insight into the mechanisms that govern egress and its functional relevance in disease requires quantitative *in vivo* methods of analysis.

Several methods have been used to quantify egress in multiple animal models *in vivo* including direct cannulation of lymphatic vessels, adoptive transfer of *ex vivo* labeled leukocytes, transdermal application of fluorescent tracers, injection of labeled particles, and *in vivo* photoconversion[17,18]. Direct cannulation of afferent mouse lymphatic vessels is difficult and limited in small animals by the volumes of fluid that can be collected. Thus, cannulation has largely been performed in large animals (*e.g.*, sheep) where such surgical manipulations are practical. These studies provide direct evidence for the presence of both lymphoid and myeloid cells in lymph[10,19,20]. Furthermore, ovine models reveal that acute and chronic inflammation increased lymphocyte presence in lymph by nearly 100-fold[10,21].

Adoptive transfer of labeled and genetically manipulated lymphocytes has importantly revealed that CCR7 is required for the egress of $CD4^+$ T cells from acutely inflamed skin[5,11], while the pretreatment of lymphocytes with the small molecule S1P receptor agonist, FTY720, only

partially inhibits their egress[10]. Interestingly, the egress of transferred lymphocytes from chronically inflamed skin is CCR7-independent[10], but may partially require CXCR4[9]. Adoptive transfer experiments, however, deliver non-physiological numbers of *ex vivo* activated and labeled lymphocytes into tissue through injection, which alters the biomechanical environment of tissues and elevated interstitial fluid pressures that open initial lymphatic capillaries and alter their transport properties[22]. As an alternative, transdermal application of fluorescein isothiocyanate (FITC) in the presence or absence of dermal irritants (*e.g.*, dibutyl phthalate, DBP) or infection[23,24] allows for the tracking of phagocytic cells that accumulate tracer and migrate to dLNs. Similarly, fluorescently labeled tumors provide a means to track phagocytic cells that have engulfed tumor material[25]. These methods have provided important insight into the mechanisms that govern DC egress[13,14,17,26,27] but are unable to track non-phagocytic lymphocytes and, interpretation can be complicated by free lymphatic drainage of soluble FITC thus labeling non-migratory, LN resident DCs.

Alternatively, intravital microscopy is a powerful tool that allows for *in vivo* tracking of physiologically relevant leukocyte populations in real time[28,29]. Used in combination with the reporter mice and antibody-based *in vivo* immunofluorescent labeling, intravital microscopy has revealed the complex spatial and temporal dynamics of immune cell trafficking, including interstitial migration[30], transmigration across the lymphatic endothelium, passage within the lymphatic lumen, and migration upon LN entry[28,31]. Broad adoption of intravital imaging techniques is limited by expense, necessary expertise for set up, and limited throughput for quantifying multiple cell types. Still, coupling quantitative methods that analyze population dynamics tissues with intravital imaging will provide additional and important mechanistic insight with respect to the mechanisms of motility and migration toward and within lymphatic capillaries[18,31,32].

Consequently, *in vivo* photoconversion has emerged as a method that allows for *in situ* labeling, independent of phagocytic activity, and for the quantification of physiological leukocyte egress (when coupled with flow cytometry) in the absence or presence of challenge. Kaede-Tg mice constitutively express a protein isolated from stony coral that exhibits green fluorescence (Kaede green) until exposed to violet light, after which it irreversibly converts to red fluorescence (Kaede red)[33]. Photoconverted cells can be tracked as they egress from peripheral tissue sites and accumulate in dLNs. This and other similar photoconvertible mouse models[34,35] have revealed important biology including constitutive egress of regulatory T cells from skin[36], CXCR4-dependent B cell egress from Peyer's patches[37], mobilization of resident memory T cells upon peptide re-challenge[38], and broad leukocyte egress from tumor microenvironments[39]. Herein, we perform a head-to-head comparison of photoconversion with transdermal FITC application in the context of cutaneous inflammation and infection to allow for direct comparison of existing data with the photoconvertible method. Furthermore, we demonstrate photoconversion in implanted tumors and describe the conversion efficiency and selective egress from tumor microenvironments. As such, we argue that further application of these methods is needed to elucidate the critical biology of leukocyte egress from tumors, which will have significant implications for interpreting intratumoral leukocyte complexity, anti-tumor immunity, and response to therapy.

Protocol

All animal protocols have been approved by the Institutional Animal Care and Use Committee at the Oregon Health & Science University.

1. Induction of Inflammation and FITC Painting of Mouse Pinna

1. In a laminar flow hood, anesthetize a C57Bl/6 mouse using vaporized isofluorane (induce at 3-5% isofluorane and maintain at 1-3% isofluorane; oxygen flow rate at 0.5-1.0 L/min). Ensure proper anesthetization by monitoring the loss of pedal reflex, involuntary movements and reduced respiratory rate.
2. Lay an ear flat with the ventral side of the ear facing upwards. Pipet 20 µL of 5% FITC solution dissolved in 1:1 acetone:dibutyl phthalate (DBP) to the ventral side of ear pinna. Allow the ear to dry for a few seconds.
3. 24 h after FITC application, euthanize the mice via carbon dioxide exposure followed by cervical dislocation. Collect the ear pinnae into PBS by separating the ears from the head using scissors. Collect the cervical dLNs and inguinal non-draining LNs into PBS using tweezers to separate the LNs from surrounding tissues. Inguinal non-draining LNs will serve as negative controls for the presence of $FITC^+$/$Kaede\ red^+$ leukocytes. Dispose of carcasses per institutional protocol.
   Note: The optimal time post photoconversion for analysis will depend on the cell type and known migratory behaviors. Dendritic cells, for example, can be detected in dLNs as early as 6 h post DBP application.

2. Induction of Inflammation and Photoconversion of Mouse Pinna

1. In a laminar flow hood, anesthetize a Kaede-Tg mouse (background C57Bl/6) by intraperitoneal injection of 80 mg/kg ketamine and 10 mg/kg xylazine dissolved in saline. Ensure proper anesthetization as described in Step 1.1.
2. Lay an ear flat with the ventral side of the ear facing upwards. Pipet 20 µL of a 1:1 acetone:DBP to the ventral side of the ear pinna. Allow the ear to dry for a few seconds.
3. After DBP application, cut a slit in a piece of aluminum foil and pull the ear through the slit to expose the ear to the violet light source. Lay the ear flat with the dorsal side facing upward using double-sided tape to secure the ear to the foil.
4. Position the ear directly under the light source, and photoconvert for 3 min using a 405 nm light source at 100 mW power.
5. 24 h after photoconversion, euthanize the Kaede-Tg mice and harvest the ear pinnae, cervical LNs, and inguinal LNs as described in Step 1.3.
   Note: In addition to considerations cited in Step 1.3, the rates of proliferation will determine the timing of analysis as the loss of Kaede red will occur in rapidly dividing cells.

3. Vaccinia Infection of Mouse Pinna and FITC Application

1. Anesthetize a C57Bl/6 mouse with vaporized isofluorane as described in Step 1.1.

2. Lay the ventral side of the ear flat. Pipet 5 x 10^6 plaque-forming units (PFU) of vaccinia virus (VacV) diluted in 10 µL of PBS onto the ear pinna. Using a 29-gauge needle, poke the pinna 25 times[40].
3. 24 h post-infection, anesthetize VacV-infected mice with isofluorane as described in Step 1.1 and pipet 20 µL 5% FITC dissolved in acetone onto the ventral side of the ear pinna. Allow the ear to dry for a few seconds.
4. 24 h after FITC application, euthanize the mice and collect the ear pinnae, cervical LNs and inguinal LNs as described in Step 1.3.
Note: FITC may be applied at any time point post infection to determine DC trafficking at various 24 h intervals. We previously reported that DC migration to dLNs is maintained at similar levels from day 1 to 3 post infection[41].

4. Vaccinia Infection of Mouse Pinna and Photoconversion.

1. Anesthetize a Kaede-Tg mouse with vaporized isofluorane as described in Step 1.1.
2. Infect the ear pinna with VacV as described in Step 3.2.
3. 24 h post-infection, anesthetize VacV-infected Kaede mice as described in Step 2.1 and perform photoconversion as described in Steps 2.3-2.4.
4. 24 h after photoconversion, euthanize the mice and harvest the ear pinnae, cervical LNs, and inguinal LNs as described in Step 1.3.
Note: As mentioned above in Step 3.4, photoconversion can be administered at any time point post infection.

5. Ear and Lymph Node Processing for Flow Cytometry

1. Create single cell suspensions of ear pinnae: peel apart the ventral and dorsal sides of the ear pinna using two pairs of tweezers and place with the inside of the ear facing down into the wells of a 24-well plate containing 1 mg/mL collagenase D and 80 U/mL DNase diluted in Hank's Buffered Saline Solution (HBSS) (containing Ca^{2+} and Mg^{2+}). Incubate at 37 °C for 30 min. Press the digested tissue through a 70 µm nylon cell strainer.
2. Create single cell suspensions from LNs: place LNs in wells of a 24-well plate containing 1 mg/mL collagenase D and 80 U/mL DNase diluted in HBSS. Tease open the lymph node capsule using two 29-gauge needles, and then incubate the lymph nodes at 37 °C for 30 min. Press the digested tissue through a 70 µm nylon cell strainer.

6. Intradermal Melanoma Tumor Implantation and Photoconversion.

1. Shave the fur from the center of the back of a Kaede-Tg mouse using an electric razor.
2. Position a 29-gauge needle in the center of the back between the left and right upper scapulae, and intradermally inject 5 x 10^5 tumor cells (diluted in 50 µL of saline) into the skin of Kaede-Tg mice. Tumors must be carefully positioned to ensure lymphatic drainage to specified lymph nodes (*i.e.*, left and right brachial LNs for tumors placed in the middle of the upper back). Avoid placing the tumor above dLN as this can result in direct photoconversion of the LNs through the skin/tumor.
3. Allow the tumors to grow to desired size (100-650 mm^3).
4. One day prior to tissue collection, anesthetize a Kaede-Tg mouse as described in 2.1 and shave any newly regrown fur around the tumor.
5. Cut a circular hole in aluminum foil and pull the tumor through to expose the tumor to the light source. Cut the hole slightly smaller than the tumor to prevent the tumor from falling back through the hole and minimize the conversion of adjacent, non-tumor skin.
6. Position the tumor directly below the light source and photoconvert for 5 min using a 405 nm light source at 200 mW power.
7. 24 h after photoconversion, euthanize the mice as described in Step 1.3. Collect the tumors, brachial dLNs, and inguinal non-draining LNs into PBS. Cut the tumors away from the surrounding skin using scissors and remove LNs as described in Step 1.3.

7. Tumor and Lymph Node Processing for Flow Cytometry

1. Create single cell suspensions from the tumors: mince the tumors with scissors into wells of a 24-well plate containing 1 mg/mL collagenase D and 80 U/mL DNase diluted in HBSS. Incubate at 37 °C for 1 h. Press the digested tissue through a 70 µm nylon strainer.
2. Create single cell suspension of lymph nodes as described in Step 5.2.

8. Antibody Staining for Flow Cytometry

1. After digesting the tissues into single cell suspensions, perform standard flow cytometry staining techniques to label the cells with markers of interest. Briefly, pipet 2 x 10^6 cells into a 96-well plate. Incubate the samples with Fc block (1 µg/mL) for 20 min on ice; wash twice with FACs buffer (1% bovine serum albumin in PBS). Add live/dead stain (diluted in PBS) to the samples and incubate for 15 min on ice; wash twice with FACs buffer. Incubate with primary antibodies (**Table of Materials**) diluted in FACs buffer for 30 min on ice; wash twice with FACs buffer.
Note: Kaede green and Kaede red fluorescence overlaps with FITC and PE fluorophores; thus, FITC and PE-conjugated antibodies cannot be used in combination with Kaede proteins.
2. After staining, run the samples on a flow cytometer. Alternatively, fix the cells with 2% PFA.

9. Flow Cytometry Analysis

1. Set the FITC (Kaede green) and PE (Kaede red) channel PMT voltages to 70-80% of the total range (center population at approximately 10^4) using *ex vivo* Kaede green or Kaede red single-color splenocytes or blood.
Note: Do not compensate for the Kaede green (FITC) and Kaede red (PE) channels as this will result in greater signal spread.
    1. To create single-color Kaede controls, collect a spleen or blood from a Kaede-Tg mouse. Lyse the red blood cells with ACK buffer, then divide the cells into two groups: unconverted Kaede green and converted Kaede red.

2. For single color Kaede red controls, suspend the cells in 1 mL of PBS and photoconvert in a 24-well plate for 5 min using a 405 nm light sources at a power of 100 mW. Use these cells to set the Kaede green (FITC) and Kaede red PMT voltages on the flow cytometer (Step 9.1).

2. Once the voltages for the Kaede proteins has been set, compensate for all other primary antibody stains using single-fluorophore labeled compensation beads per manufacturer's instructions.
3. Run the samples on a flow cytometer to collect data.
   Note: The Kaede protein is continually being produced by the cells. This means that 24 h after photoconversion, converted cells will be double positive for Kaede green and Kaede red as newly synthesized Kaede (green) protein has accumulated in the cell.
4. Analyze the data using FlowJo software or a similar software.

Representative Results

We first sought to replicate photoconversion results published in the literature to evaluate the efficiency and determine the associated inflammation in the mouse skin. The ear pinna was exposed to 100 mW violet light (405 nm) for 3 min as previously described[33]. Single cell suspensions generated from the ear skin or cervical dLNs immediately following the exposure revealed a 78% conversion efficiency of all $CD45^+$ leukocytes in the skin with no converted cells observed in dLNs (**Figure 1A**). To evaluate the inflammatory response associated with photoconversion, we quantified the numbers of infiltrating $CD45^+$ leukocytes in converted ears 0 and 24 h post conversion (**Figure 1B**) and acute changes in vascular permeability as measured by Mile's Assay[42] (**Figure 1C**). Briefly, 200 µL of 0.5% Evans Blue was intravascularly injected 2 h after photoconversion. The ears were collected 30 min after the injection and Evans Blue was extracted with formamide for 24 h at 55°C (absorbance read at 610 nm[42]). Both $CD45^+$ infiltrates (24 h) and vascular leak (2 h) were significantly increased following the photoconversion, indicating that even at this short exposure, photoconversion itself may impact the tissue-specific inflammatory response. Comparison to $CD45^+$ infiltrates (**Figure 1B**) and vascular leak (1.4 µg/ear ±0.75) in VacV infected ears 24 h post infection[41] provides context for the extent of the inflammation caused by violet light (0.08 µg/ear ± 0.01).

While several models have been used in various studies to track the leukocyte egress from non-lymphoid, peripheral tissues, it is unclear how these methods compare in their ability to track specific populations as they exit the skin. Consequently, we decided to perform a direct head-to-head comparison of two commonly used methods to track DC egress to LNs, FITC paint and *in vivo* photoconversion, in order to evaluate the efficiency and specificity of each method for quantitative analysis of DC egress at steady state, during cutaneous inflammation, and from infected skin. For each analysis, the skin was subjected to transdermal FITC application or exposed to 100 mW 405 nm light for 3 min. LN DC populations were defined as $CD3\varepsilon^-CD19^-MHCII^+CD11c^+$ and further stratified into 1) $MHCII^{hi}CD11c^{int}$ DCs, which enriches for migratory DCs (mDCs) both $CD103^+$ BATF3-dependent cross-presenting DCs, and $CD11b^+$ dermal DCs; and 2) $MHCII^{int}CD11c^{hi}$ DCs, which enriches for resident DCs (rDCs) including $CD8\alpha^+$ BATF3-dependent cross-presenting DCs (**Figure 2A**). 24 h after either FITC application or photoconversion, the labeled cells were readily detectable in draining but not non-draining LNs (**Figure 2B**). To quantify the extent of DC migration to LNs and simultaneously determine the specificity of the method for labeling migrating populations and not resident LN populations, we quantified labeled mDCs and rDCs at steady state, 24 h following the application of DBP, and 48 h following VacV scarification (**Figure 2C**). While both photoconversion (Kaede) and FITC labeled mDCs in all conditions, we observed more FITC-labeled than Kaede-labeled mDCs in dLNs, with the exception of VacV infection where the two methods quantified a similar level of egress. Furthermore, in the context of DBP, FITC additionally labeled rDC populations where photoconversion remained specific to mDCs (**Figure 2C**). Using both of these methods, we observed the egress of approximately 200 DCs from VacV infected skin and importantly noted that this level of egress recapitulates previously published findings using transdermal FITC application by Loo *et al.*[41]. Thus, depending on inflammatory context, transdermal FITC application may increase the numbers of labeled DCs detected in dLNs and result in non-specific labeling of non-migratory LN-resident DC populations, while photoconversion specifically identifies DCs falling into a mDC population.

Kaede-Tg mice have been used to quantify the leukocyte retention in[5,33,43] and egress from[5,6,35,38] cutaneous, mucosal, and lymphoid tissues under steady state and inflamed conditions and applied to tumors only in a single publication where the tumors were implanted intradermal into the mouse ears and photoconverted at small volumes[39]. Thus, we sought to evaluate the utility of *in vivo* photoconversion for the quantification of leukocyte egress from established, large primary tumors to enable further immunological hypothesis testing. First, we implanted MC38 tumor cells intradermally into Kaede-Tg mice between the left and right scapulae. Implantable tumor models enable precise positioning of the tumors to ensure lymphatic drainage to known LNs; tumors placed in the skin of the upper back primarily drain to left and right brachial LNs. After reaching 100 - 150 mm^3, the tumors were photoconverted (10 min, 200 mW) and the tumors and dLNs harvested immediately after photoconversion. Analysis by flow cytometry revealed significant conversion of intratumoral $CD45^+$ cells from Kaede $green^+$ to Kaede red^+ (69%; **Figure 3A**), while importantly, dLNs remained negative for Kaede red^+ cells. Immunofluorescence microscopy of photoconverted YUMM 1.7 tumors revealed that photoconversion penetrates deep into the tumor tissue (>1 mm; **Figure 3B**). Interestingly, the skin and vascular cells express high levels of the Kaede protein leading to high photoconversion efficiency of these cell types as seen in **Figure 3B**. This high Kaede red expression makes it difficult to identify the immune cells (both unconverted and converted) using immunofluorescence microscopy.

Given our particular interest in melanoma immunology, we next evaluated the effect of both tumor size and melanin on photoconversion efficiency using various implantable murine tumor cell lines: MC38 (unpigmented colorectal cancer line), B16.F10 (melanin-producing melanoma line), YUMM 1.1 (unpigmented melanoma line), and YUMM 1.7 (unpigmented melanoma line)[44]. Each of these lines were implanted intradermal into Kaede-Tg mice and photoconverted, as described above at various tumor volumes (50 - 650 mm^3). The tumors were harvested immediately following the photoconversion and evaluated for the presence of Kaede red $CD45^+$ leukocytes by flow cytometry. Interestingly, the photoconversion efficiency of $CD45^+$ leukocytes varied significantly across the tumor types and sizes (**Figure 3C**). $CD45^+$ leukocytes within small (50 - 150 mm^3) YUMM 1.7 and YUMM 1.1 tumors demonstrated the most efficient photoconversion at 80% and 60%, respectively. As the volumes increased for these tumors, the conversion efficiencies decreased to around 50% for large tumors (> 600 mm^3). Melanin had a striking impact on photoconversion efficiency: maximum photoconversion for $CD45^+$ cells within melanin-producing B16.F10 tumors was only about 30% and dropped to 10% as the tumors reached volumes of 400 mm^3. Interestingly, analysis of intratumoral $CD8^+$ T cells revealed photoconversion efficiency for these cells at nearly 80 - 90% in small tumors regardless of melanin production (**Figure 3D**). For unpigmented tumors, $CD8^+$ T cell conversion remained high even as the tumors reached large volumes, but decreased significantly with the size when the melanin was present. As such, the utility of B16.F10 murine melanomas, and other melanin-producing melanoma lines, may be limited to small tumors (50 mm^3), which is consistent with the biological function of melanin in absorbing light. To evaluate the inflammatory response associated with the photoconversion of tumors, we quantified the number of $CD45^+$ cells in unconverted tumors and converted tumors 24 h post photoconversion (**Figure 3E**). We saw no significant difference in the total numbers of $CD45^+$ cells detected in the tumors 24 h following the photoconversion compared to unconverted tumors.

We next quantified the leukocyte egress from tumor microenvironments using Kaede-Tg mice, which allows for the interrogation of trafficking behavior of both myeloid and lymphoid cell types. MC38 or YUMM 1.7 tumor cells were intradermally implanted into Kaede-Tg mice. The tumors were photoconverted once the volumes reached between 100 - 150 mm^3 (5 min, 200 mW); brachial dLNs and inguinal non-draining LNs were collected 24 h after the photoconversion. Intratumoral leukocyte populations were quantified from MC38 and YUMM 1.7 tumors implanted into control C57Bl/6 mice and collected once the tumors reached 100 - 150 mm^3. We evaluated the leukocyte complexity within the tumors and egressed populations by flow cytometry: T cells ($CD3\varepsilon^+CD4^{+/-}CD8^{+/-}$), B cells ($CD3\varepsilon^-CD19^+$), DCs ($CD11c^+MHCII^+CD11b^{+/-}$), neutrophils ($CD11b^+MHCII^-Ly6G^+$), macrophages ($CD11b^+MHCII^+F4/80^+$), and inflammatory monocytes ($CD11b^+Ly6G^-Ly6C^+$; **Figure 4A**). Using this same gating scheme, we evaluated the percent of each leukocyte population in dLNs that expressed Kaede red indicating previous residence in tumor microenvironments (**Figure 4B**). Interestingly, while both MC38 (**Figure 4C**) and YUMM 1.7 (**Figure 4D**) tumors were mainly infiltrated with the myeloid cells (monocytes, DCs, and macrophages), approximately 50% of the cells that had egressed from both tumor types were T lymphocytes (both $CD4^+$ and $CD8^+$). In addition to T cells, we also observed DCs, B cells, and monocytes within egressed populations from the tumors but macrophages and neutrophils were not detected from either tumor type. Altogether, this data demonstrates the utility of Kaede-Tg photoconvertible mice for tracking multiple leukocyte lineages in an endogenous setting. Furthermore, our analysis indicates that egress is a selective, active process that may have significant implications for determining intratumoral leukocyte complexity.

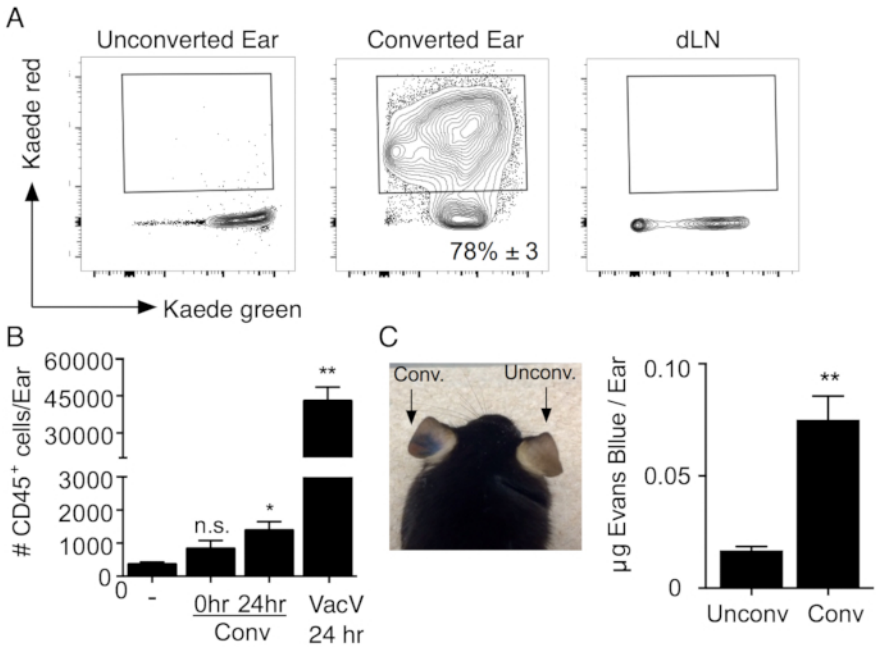

Figure 1: Photoconversion efficiency and associated inflammation in murine skin. Murine dermis was photoconverted for 3 min at 100 mW (405 nm light). **(A)** Representative flow plots depicting photoconverted (Kaede red^+) $CD45^+$ cells from an unconverted and converted ear and cervical dLN immediately following photoconversion. Populations were pre-gated on live, $CD45^+$ single cells. **(B)** Enumeration of total $CD45^+$ cells in unconverted ears (-), ears collected immediately following photoconversion, ears collected 24 h after photoconversion, and ears collected 24 h after VacV infection (n = 3). **(C)** A Mile's assay was performed to quantify vascular leakiness immediately following the exposure to 405 nm light (3 min, 100 mW). Representative image of leakage in ear skin (left) and quantification of extracted dye (right) (n=3). Error bars represent SEM. *p<0.05 and **p<0.01. Please click here to view a larger version of this figure.

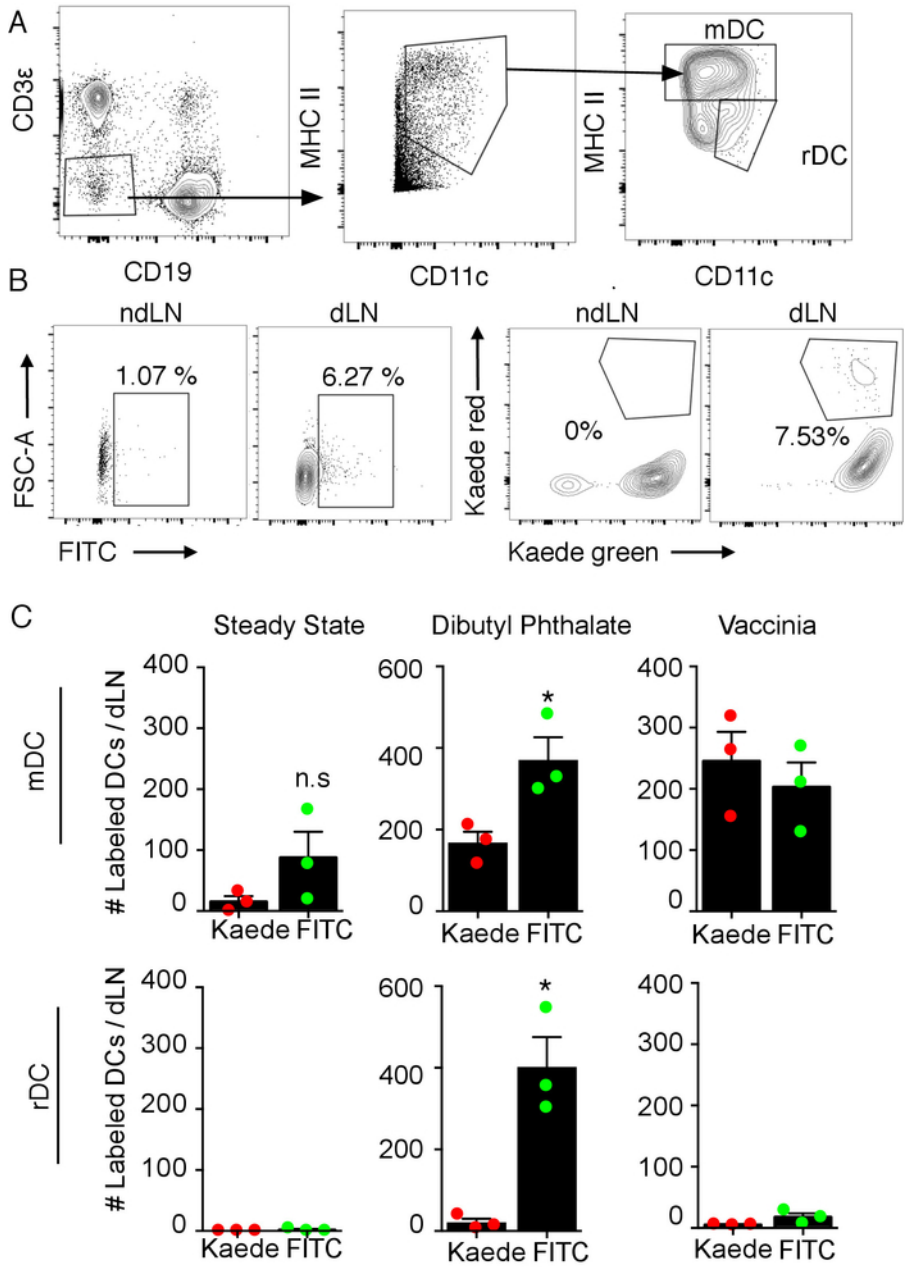

Figure 2: DC egress from naïve, inflamed, and infected skin. (A) Gating scheme to identify migratory DCs (mDCs; MHCII^{hi}CD11c^{int}) and resident DCs (rDCs; MHCII^{hi}CD11c^{hi}). **(B)** Representative flow plots indicating FITC^{+} or Kaede red^{+} DCs, pre-gated on mDCs, from the mice infected with VacV (dLN) or contralateral non-draining LN controls. **(C)** Quantification of the numbers of Kaede red^{+} and FITC^{+} mDCs and rDCs in dLNs of steady state, DBP-inflamed (24 h post application), and VacV infected skin (48 h post infection). Error bars represent SEM. Please click here to view a larger version of this figure.

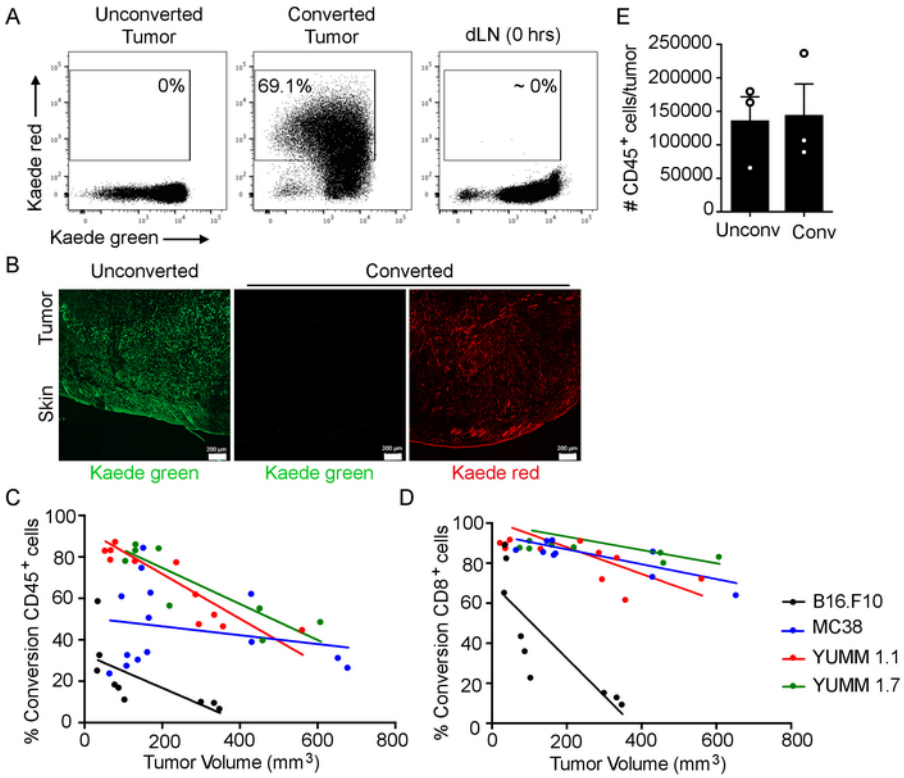

Figure 3: Photoconversion efficiency in tumor microenvironments. Tumors were photoconverted for 10 min at 200 mW (405 nm light). **(A)** Representative flow plots of Kaede green and Kaede red in unconverted and converted MC38 tumors and brachial dLN immediately following photoconversion. Populations were pre-gated on live, $CD45^+$ single-cells. **(B)** Immunofluorescence microcopy of frozen, OCT-embedded YUMM 1.7 tumors both unconverted and photoconverted. Scale bar = 200 µm. **(C)** Conversion efficiency of $CD45^+$ leukocytes and **(D)** $CD8^+$ lymphocytes in melanin-producing (B16.F10) and unpigmented (MC38, YUMM 1.1, YUMM 1.7). Each point represents a single mouse. **(E)** Enumeration of total $CD45^+$ cells in unconverted tumors and photoconverted tumors collected 24 h after photoconversion (n = 3). Error bars represent SEM. Please click here to view a larger version of this figure.

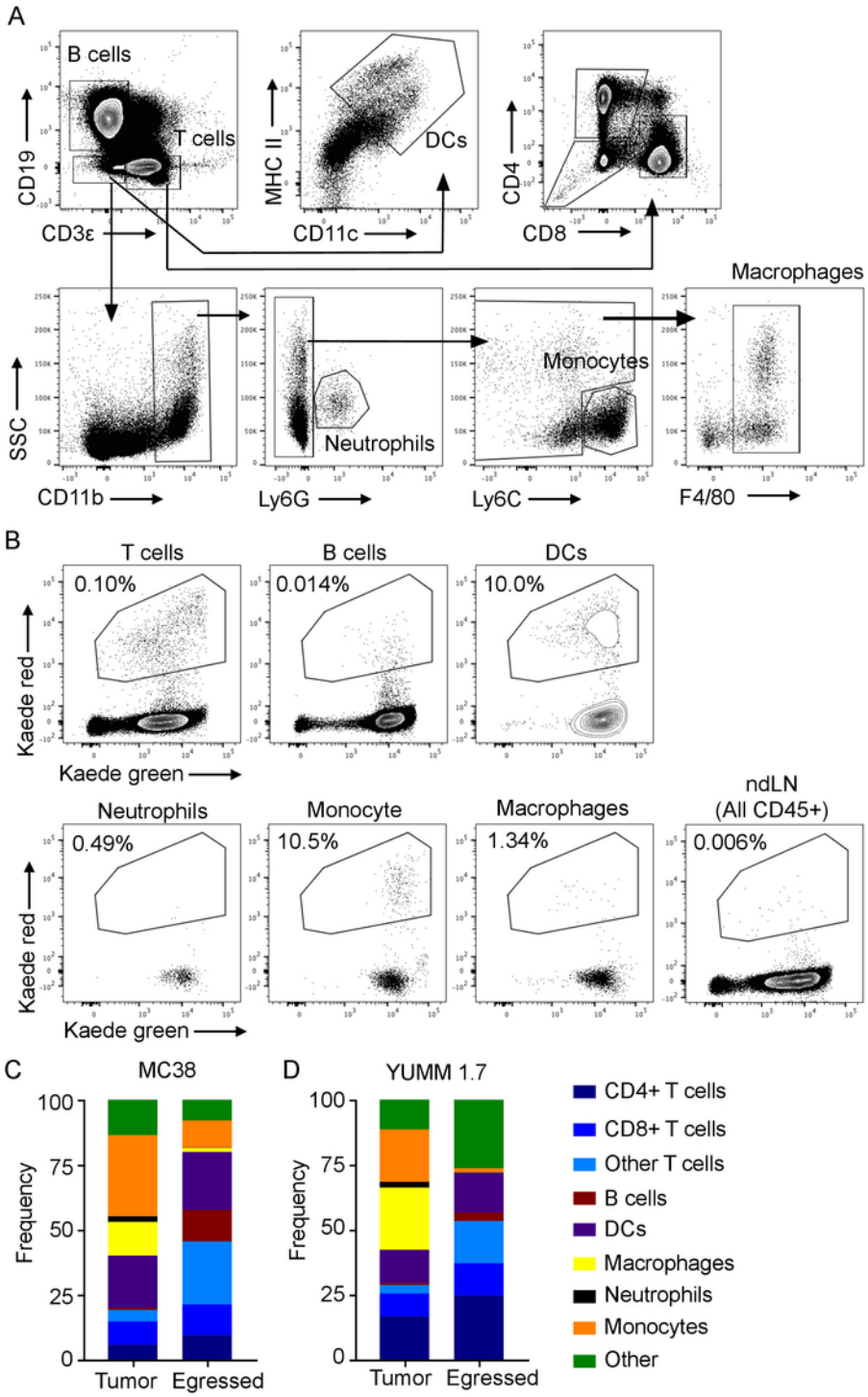

Figure 4: Leukocyte egress from tumor microenvironments is selective. (A) Gating scheme for identifying myeloid and lymphoid populations in MC38 dLNs. **(B)** Representative flow plots identifying Kaede red^{+} cells among myeloid and lymphoid cells in MC38 dLNs 24 h after photoconversion. Percentages in flow plots indicate the frequency of Kaede red^{+} cells within the indicated parent leukocyte population in LNs. **(C, D)** Relative proportions of intratumoral (% of CD45^{+} cells) and egressed (% Kaede red^{+} cells; brachial dLNs) leukocytes from MC38 (**C**, n = 3) and YUMM 1.7 (**D**, n = 4) tumors. Please click here to view a larger version of this figure.

Discussion

Although the leukocyte egress from peripheral, non-lymphoid tissues is critical for the initiation and resolution of immune responses, the molecular mechanisms that govern egress are poorly understood. This gap in knowledge is largely due to ready availability of tools for the quantification *in vivo*. Here, we describe the use of photoconvertible mice (Kaede-Tg) to quantify endogenous leukocyte egress from the skin

and tumors and provide a direct head-to-head comparison with FITC paint in inflammatory and infection models. We demonstrate that while both models track endogenous DC populations, free drainage of FITC and poor uptake by non-phagocytic cells limits the utility of FITC paint for broad analysis of myeloid and lymphoid egress from peripheral, non-lymphoid tissues including tumors. Moreover, we present the data that indicates the egress from the tumors is selective rather than stochastic thus confirming findings presented by Torcellan *et al.*[39]. Further investigation of the mechanisms governing leukocyte egress from tumors may reveal novel insight into tumor-associated inflammation and immunity.

We first evaluated the efficiency of photoconversion in murine skin and its effect on local inflammation when using settings reported in literature. The exposure of ears to violet light for 3 min at 100 mW power resulted in efficient photoconversion of $CD45^+$ cells within the ear skin (78%) with no conversion in downstream dLNs. Reports in the literature demonstrate the 3-5 min exposure is optimal for cutaneous tissues[5,33,38]. However, this exposure led to increased numbers of $CD45^+$ cells in the ear pinna 24 h following the conversion and vascular leakage indicating that photoconversion at these settings in ear skin induces local inflammation, which should be considered when interpreting data. We next sought to directly compare DC trafficking to LNs using both Kaede photoconversion and the more broadly utilized FITC paint assay[23,24] at steady-state, during DBP-induced inflammation, and from VacV infected ears. We observed elevated labeling in FITC treated as compared to photoconverted skin at steady state and following DBP treatment. Application of free FITC to skin can result in direct drainage via lymphatic vessels to draining LNs where resident DC populations, that do not migrate (*e.g.*, $CD8\alpha^+$ DCs), sample FITC. Consistent with this, we observed significant numbers of rDCs with FITC label when treated with the irritant DBP. In contrast, Kaede red-labeled DCs were only observed in the mDC population following the photoconversion indicating that photoconversion provides a more specific way to label mDCs. Even within the mDC population, however, we observed quantitatively more labeled mDCs when using FITC over photoconversion. While this may also be explained by free FITC drainage, it is possible that the differences in the period of labeling, where the photoconversion can only label DCs currently resident in skin while FITC remains in the skin for the duration of the 24 h period, accounts for the differences in observed mDC egress. Interestingly, in the context of viral infection, both photoconversion and FITC application measured relatively equal levels of mDC egress and few $FITC^+$ rDCs in the LNs draining VacV-infected ears. We recently reported that lymphatic drainage is significantly reduced following VacV infection, and thus the viral-induced reduction in lymphatic transport may improve the specificity of FITC paint and reduced labeling of LN resident DC populations[31]. Importantly, this work also highlights the fact that within the mDC population ($CD3\varepsilon^-CD19^-MHCII^{hi}CD11c^{int}$), the number of DCs that have actively migrated within 24 h is a minor population and thus total mDC numbers are not a good surrogate for active migration[41]. Finally, it is interesting to note that we consistently quantify mDC egress at around 200 cells for any given 24 h period following VacV infection[41], while 1500-2000 DCs egress from tumor microenvironments. Given the tremendous efficacy of VacV as a vaccine platform, particularly when applied by scarification[45,46,47], it is interesting to speculate that it is the quality of the DC and perhaps the type of DC presenting antigen, rather than the quantity, that determines robust protective immunity.

Leukocyte egress from tumor microenvironments, beyond DCs[25,48], remains a poorly investigated area. Although the tumors are considered chronically inflamed microenvironments, whether similar mechanisms regulate cellular egress from non-malignant and malignant tissues remains unknown. Furthermore, whether leukocyte egress from tumors is stochastic or rather selective will have significant implications for interpreting leukocyte accumulation and retention in tumor microenvironments. As such, leukocyte egress from tumors may be crucial to understanding how tumors evade immune surveillance and lead to novel strategies for immunotherapy. Here we apply the photoconvertible Kaede-Tg model to study leukocyte egress from implantable cutaneous tumors, where FITC paint would be insufficient to broadly label both myeloid and lymphoid populations. Initial studies revealed that photoconversion efficiency in implanted tumors was dependent both upon tumor size and melanin. While photoconversion efficiency rapidly drops off as tumors grow when melanin is present (B16.F10), non-pigmented tumor lines such as the YUMM and MC38 tumors exhibit more stable conversion efficiency across tumor sizes tested. Interestingly, we observed improved conversion efficiency in the $CD8^+$ T cell compartment compared to $CD45^+$ cells, which declined as tumors increased in size. There are likely several factors contributing to this observation. First, the location within a tumor will impact the exposure and thus the conversion efficiency of particular cell types. T cells are frequently found restricted to the skin-tumor interface in implantable tumor models and thus may be more readily photoconverted relative to myeloid cells infiltrating the tumor parenchyma. Secondly, not all leukocytes express the same levels of the Kaede protein[49] and thus may not all be equally detected by flow cytometry; this may lead to lower observed percentages of photoconversion when analyzing a more heterogeneous cell population such as all $CD45^+$ cells. Finally, it is important to note that data presented in **Figure 3** was generated following 10 min of violet light exposure. This initial exposure time was chosen based on reports in the literature citing photoconversion times for various organs including skin, LNs, mucosal tissues, and tumors[5,6,33,35,39,43]. The only other study employing the photoconvertible system in tumors, photoconversion was performed for 20 min[39]. Further optimization in our hands revealed improved efficiency with a shortened exposure time of 5 min for both small and large volumes. It is likely that prolonged exposure leads to photobleaching of Kaede fluorescence, and as such, our reported conversion efficiencies may be underestimates. Prolonged exposure may also lead to increased photoconversion-associated inflammation and confound study results. Tumors photoconverted for 5 min demonstrated no significant difference in the number of intratumoral $CD45^+$ cells 24 h after photoconversion compared to unconverted tumors. Additionally, the tumors photoconverted for 5 min demonstrated measurable and reproducible egress for both myeloid and lymphoid populations. Consequently, individual optimization within specific tissues or tumors of interest is necessary to achieve optimal results.

Lastly, we used *in situ* photoconversion to quantify endogenous leukocyte egress from tumors implanted into Kaede-Tg mice. Using two different implantable, non-pigmented tumor models we observed significant egress of DCs, T cells, and monocytes. Consistent with recently published work[39], both $CD4^+$ and $CD8^+$ T cells egressed from tumor microenvironments along with a significant number of double negative $CD3\varepsilon^+$ T cells. At least, one component of this population may be gamma delta T cells as previously described[39], though the functional significance of this observation remains to be determined. Importantly, when we compared the proportions of leukocytes egressing from tumors to the relative proportions of leukocytes present within the tumor microenvironments, we observed leukocyte enrichment in egressed populations relative to intratumoral pools in both models indicating selective leukocyte egress. Notably, macrophages and neutrophils were absent in egressed populations, though both cell types have been described to egress under inflamed and infected conditions[2,50,51,52,53,54] and are significant contributors to intratumoral leukocyte repertoires[39,55,56]. Thus, the leukocyte egress from the tumors can be quantified using photoconvertible models, is not stochastic but rather a regulated process, and remains an important and understudied biology with significant implications for understanding inflammatory and immune dynamics in tumor microenvironments at steady state and in response to therapy.

Disclosures

The authors have no conflicts to disclose.

Acknowledgements

The authors would like to thank Dr. Marcus Bosenberg for providing YUMM 1.1 and YUMM 1.7 murine melanoma lines and Dr. Deborah J. Fowell for providing B6.Cg-Tg(CAG-tdKaede)15Utr mice in agreement with RIKEN BRC through the National Bio-Resource of the MEXT, Japan.

References

1. Banchereau, J., & Steinman, R. M. Dendritic cells and the control of immunity. *Nature.* **392** (6673), 245-252, (1998).
2. Hampton, H. R., Bailey, J., Tomura, M., Brink, R., & Chtanova, T. Microbe-dependent lymphatic migration of neutrophils modulates lymphocyte proliferation in lymph nodes. *Nature Communications.* **6** 7139, (2015).
3. D'Alessio, S. *et al.* VEGF-C-dependent stimulation of lymphatic function ameliorates experimental inflammatory bowel disease. *Journal of Clinical Investigation.* **124** (9), 3863-3878, (2014).
4. Debes, G. F. *et al.* Chemokine receptor CCR7 required for T lymphocyte exit from peripheral tissues. *Nature Immunology.* **6** (9), 889-894, (2005).
5. Bromley, S. K., Yan, S., Tomura, M., Kanagawa, O., & Luster, A. D. Recirculating memory T cells are a unique subset of CD4+ T cells with a distinct phenotype and migratory pattern. *Journal of Immunology.* **190** (3), 970-976, (2013).
6. Tomura, M. *et al.* Activated regulatory T cells are the major T cell type emigrating from the skin during a cutaneous immune response in mice. *Journal of Clinical Investigation.* **120** (3), 883-893, (2010).
7. Tomura, M., Itoh, K., & Kanagawa, O. Naive CD4+ T lymphocytes circulate through lymphoid organs to interact with endogenous antigens and upregulate their function. *Journal of Immunology.* **184** (9), 4646-4653, (2010).
8. Jennrich, S., Lee, M. H., Lynn, R. C., Dewberry, K., & Debes, G. F. Tissue exit: a novel control point in the accumulation of antigen-specific CD8 T cells in the influenza a virus-infected lung. *Journal of Virology.* **86** (7), 3436-3445, (2012).
9. Geherin, S. A., Wilson, R. P., Jennrich, S., & Debes, G. F. CXCR4 is dispensable for T cell egress from chronically inflamed skin via the afferent lymph. *PLoS One.* **9** (4), e95626, (2014).
10. Brown, M. N. *et al.* Chemoattractant receptors and lymphocyte egress from extralymphoid tissue: changing requirements during the course of inflammation. *Journal of Immunology.* **185** (8), 4873-4882, (2010).
11. Bromley, S. K., Thomas, S. Y., & Luster, A. D. Chemokine receptor CCR7 guides T cell exit from peripheral tissues and entry into afferent lymphatics. *Nature Immunology.* **6** (9), 895-901, (2005).
12. Gomez, D., Diehl, M. C., Crosby, E. J., Weinkopff, T., & Debes, G. F. Effector T Cell Egress via Afferent Lymph Modulates Local Tissue Inflammation. *Journal of Immunology.* **195** (8), 3531-3536, (2015).
13. Ohl, L. *et al.* CCR7 governs skin dendritic cell migration under inflammatory and steady-state conditions. *Immunity.* **21** (2), 279-288, (2004).
14. Kabashima, K. *et al.* CXCL12-CXCR4 engagement is required for migration of cutaneous dendritic cells. *American Journal of Pathology.* **171** (4), 1249-1257, (2007).
15. Cyster, J. G., & Schwab, S. R. Sphingosine-1-phosphate and lymphocyte egress from lymphoid organs. *Annual Review of Immunology.* **30** 69-94, (2012).
16. Matloubian, M. *et al.* Lymphocyte egress from thymus and peripheral lymphoid organs is dependent on S1P receptor 1. *Nature.* **427** (6972), 355-360, (2004).
17. Teijeira, A., Rouzaut, A., & Melero, I. Initial afferent lymphatic vessels controlling outbound leukocyte traffic from skin to lymph nodes. *Frontiers in Immunology.* **4** 433, (2013).
18. Hunter, M. C., Teijeira, A., & Halin, C. T Cell Trafficking through Lymphatic Vessels. *Frontiers in Immunology.* **7** 613, (2016).
19. Bujdoso, R., Hopkins, J., Dutia, B. M., Young, P., & McConnell, I. Characterization of sheep afferent lymph dendritic cells and their role in antigen carriage. *Journal of Experimental Medicine.* **170** (4), 1285-1301, (1989).
20. Young, A. J. The physiology of lymphocyte migration through the single lymph node in vivo. *Seminars in Immunology.* **11** (2), 73-83, (1999).
21. Seabrook, T. *et al.* The traffic of resting lymphocytes through delayed hypersensitivity and chronic inflammatory lesions: a dynamic equilibrium. *Seminars in Immunology.* **11** (2), 115-123, (1999).
22. Swartz, M. A. *et al.* Mechanics of interstitial-lymphatic fluid transport: theoretical foundation and experimental validation. *Journal of Biomechanics.* **32** (12), 1297-1307, (1999).
23. Macatonia, S. E., Knight, S. C., Edwards, A. J., Griffiths, S., & Fryer, P. Localization of antigen on lymph node dendritic cells after exposure to the contact sensitizer fluorescein isothiocyanate. Functional and morphological studies. *Journal of Experimental Medicine.* **166** (6), 1654-1667, (1987).
24. Robbiani, D. F. *et al.* The leukotriene C(4) transporter MRP1 regulates CCL19 (MIP-3beta, ELC)-dependent mobilization of dendritic cells to lymph nodes. *Cell.* **103** (5), 757-768, (2000).
25. Roberts, E. W. *et al.* Critical Role for CD103(+)/CD141(+) Dendritic Cells Bearing CCR7 for Tumor Antigen Trafficking and Priming of T Cell Immunity in Melanoma. *Cancer Cell.* **30** (2), 324-336, (2016).
26. Forster, R. *et al.* CCR7 coordinates the primary immune response by establishing functional microenvironments in secondary lymphoid organs. *Cell.* **99** (1), 23-33, (1999).
27. Johnson, L. A., & Jackson, D. G. The chemokine CX3CL1 promotes trafficking of dendritic cells through inflamed lymphatics. *Journal of Cell Science.* **126** (Pt 22), 5259-5270, (2013).
28. Teijeira, A. *et al.* T Cell Migration from Inflamed Skin to Draining Lymph Nodes Requires Intralymphatic Crawling Supported by ICAM-1/LFA-1 Interactions. *Cell Reports.* **18** (4), 857-865, (2017).
29. Kilarski, W. W. *et al.* Intravital immunofluorescence for visualizing the microcirculatory and immune microenvironments in the mouse ear dermis. *PLoS One.* **8** (2), e57135, (2013).

30. Overstreet, M. G. *et al.* Inflammation-induced interstitial migration of effector CD4(+) T cells is dependent on integrin alphaV. *Nature Immunology.* **14** (9), 949-958, (2013).
31. Russo, E. *et al.* Intralymphatic CCL21 Promotes Tissue Egress of Dendritic Cells through Afferent Lymphatic Vessels. *Cell Reports.* **14** (7), 1723-1734, (2016).
32. Steven, P., Bock, F., Huttmann, G., & Cursiefen, C. Intravital two-photon microscopy of immune cell dynamics in corneal lymphatic vessels. *PLoS One.* **6** (10), e26253, (2011).
33. Tomura, M. *et al.* Monitoring cellular movement in vivo with photoconvertible fluorescence protein "Kaede" transgenic mice. *Proceedings of the National Academy of Sciences of the USA.* **105** (31), 10871-10876, (2008).
34. Shand, F. H. *et al.* Tracking of intertissue migration reveals the origins of tumor-infiltrating monocytes. *Proceedings of the National Academy of Sciences of the USA.* **111** (21), 7771-7776, (2014).
35. Tomura, M. *et al.* Tracking and quantification of dendritic cell migration and antigen trafficking between the skin and lymph nodes. *Scientific Reports.* **4** 6030, (2014).
36. Moran, A. E. *et al.* T cell receptor signal strength in Treg and iNKT cell development demonstrated by a novel fluorescent reporter mouse. *Journal of Experimental Medicine.* **208** (6), 1279-1289, (2011).
37. Schmidt, T. H., Bannard, O., Gray, E. E., & Cyster, J. G. CXCR4 promotes B cell egress from Peyer's patches. *Journal of Experimental Medicine.* **210** (6), 1099-1107, (2013).
38. Beura, L. K. *et al.* T Cells in Nonlymphoid Tissues Give Rise to Lymph-Node-Resident Memory T Cells. *Immunity.* **48** (2), 327-338 e325, (2018).
39. Torcellan, T. *et al.* In vivo photolabeling of tumor-infiltrating cells reveals highly regulated egress of T-cell subsets from tumors. *Proceedings of the National Academy of Sciences of the USA.* **114** (22), 5677-5682, (2017).
40. Khan, T. N., Mooster, J. L., Kilgore, A. M., Osborn, J. F., & Nolz, J. C. Local antigen in nonlymphoid tissue promotes resident memory CD8+ T cell formation during viral infection. *Journal of Experimental Medicine.* **213** (6), 951-966, (2016).
41. Loo, C. P. *et al.* Lymphatic Vessels Balance Viral Dissemination and Immune Activation following Cutaneous Viral Infection. *Cell Reports.* **20** (13), 3176-3187, (2017).
42. Radu, M., & Chernoff, J. An in vivo assay to test blood vessel permeability. *Journal of Visualized Experiments.* (73), e50062, (2013).
43. Morton, A. M. *et al.* Endoscopic photoconversion reveals unexpectedly broad leukocyte trafficking to and from the gut. *Proceedings of the National Academy of Sciences of the USA.* **111** (18), 6696-6701, (2014).
44. Meeth, K., Wang, J. X., Micevic, G., Damsky, W., & Bosenberg, M. W. The YUMM lines: a series of congenic mouse melanoma cell lines with defined genetic alterations. *Pigment Cell Melanoma Research.* **29** (5), 590-597, (2016).
45. Demkowicz, W. E., Jr., Littaua, R. A., Wang, J., & Ennis, F. A. Human cytotoxic T-cell memory: long-lived responses to vaccinia virus. *Journal of Virology.* **70** (4), 2627-2631, (1996).
46. Stewart, A. J., & Devlin, P. M. The history of the smallpox vaccine. *Journal of Infection.* **52** (5), 329-334, (2006).
47. Hammarlund, E. *et al.* Duration of antiviral immunity after smallpox vaccination. *Nature Medicine.* **9** (9), 1131-1137, (2003).
48. Lund, A. W. *et al.* Lymphatic vessels regulate immune microenvironments in human and murine melanoma. *Journal of Clinical Investigation.* **126** (9), 3389-3402, (2016).
49. Tomura, M., & Kabashima, K. Analysis of cell movement between skin and other anatomical sites in vivo using photoconvertible fluorescent protein "Kaede"-transgenic mice. *Methods in Molecular Biology.* **961** 279-286, (2013).
50. Bellingan, G. J., Caldwell, H., Howie, S. E., Dransfield, I., & Haslett, C. In vivo fate of the inflammatory macrophage during the resolution of inflammation: inflammatory macrophages do not die locally, but emigrate to the draining lymph nodes. *Journal of Immunology.* **157** (6), 2577-2585, (1996).
51. Gautier, E. L., Ivanov, S., Lesnik, P., & Randolph, G. J. Local apoptosis mediates clearance of macrophages from resolving inflammation in mice. *Blood.* **122** (15), 2714-2722, (2013).
52. Abadie, V. *et al.* Neutrophils rapidly migrate via lymphatics after Mycobacterium bovis BCG intradermal vaccination and shuttle live bacilli to the draining lymph nodes. *Blood.* **106** (5), 1843-1850, (2005).
53. Beauvillain, C. *et al.* CCR7 is involved in the migration of neutrophils to lymph nodes. *Blood.* **117** (4), 1196-1204, (2011).
54. Rigby, D. A., Ferguson, D. J., Johnson, L. A., & Jackson, D. G. Neutrophils rapidly transit inflamed lymphatic vessel endothelium via integrin-dependent proteolysis and lipoxin-induced junctional retraction. *Journal of Leukocyte Biology.* **98** (6), 897-912, (2015).
55. Hanahan, D., & Coussens, L. M. Accessories to the crime: functions of cells recruited to the tumor microenvironment. *Cancer Cell.* **21** (3), 309-322, (2012).
56. Binnewies, M. *et al.* Understanding the tumor immune microenvironment (TIME) for effective therapy. *Nature Medicine.* **24** (5), 541-550, (2018).

